(1993); T. Okubo, *Langmuir* **10**, 1695 (1994).
4. G. Y. Onoda, *Phys. Rev. Lett.* **55**, 226 (1985); D. H. Van Winkle and C. A. Murray, *Phys. Rev. A* **34**, 562 (1986); R. G. Freeman *et al.*, *Science* **267**, 1629 (1995).
5. A. McPherson, *Preparation and Analysis of Protein Crystals* (Wiley, New York, 1982); G. Kolata, *Science* **229**, 370 (1985); F. Rosenberger, *J. Cryst. Growth* **76**, 618 (1986).
6. T. W. Healy, *Adv. Chem. Ser.* **234**, 146 (1994).
7. G. Vigil, Z. Xu, S. Steinberg, J. Israelachvili, *J. Colloid Interface Sci.* **165**, 367 (1994).
8. P. Richetti, J. Prost, P. Barois, *J. Phys. Lett.* **45**, L-1137 (1984); F. Richetti, J. Prost, N. A. Clark, in *Physics of Complex and Supermolecular Fluids*, S. A. Safran and N. A. Clark, Eds. (Wiley, New York, 1987), p. 387.
9. M. Giersig and P. Mulvaney, *J. Phys. Chem.* **97**, 6334 (1993); *Langmuir* **9**, 3408 (1993). These researchers observed the formation of 2D colloidal clusters and monolayers; however, they did not postulate a mechanism for the lateral attraction of particles on the electrode surface.
10. J. Turkevich, P. C. Stevenson, J. Hillier, *Discuss. Faraday Soc.* **11**, 55 (1951).
11. Extensive 2D clustering of these gold particles is not possible through capillary aggregation mechanisms that occur during drying. These mechanisms always result in patchy, more irregular structures, as has been demonstrated by J. Liu, W. Y. Shih, M. Sarikaya, and I. A. Aksay [*Phys. Rev. A* **41**, 3206 (1990)] and control experiments performed by us.
12. J. O. Bockris and S. U. M. Khan, *Surface Electrochemistry: A Molecular Level Approach* (Plenum, New York, 1993).
13. V. G. Levich, *Physicochemical Hydrodynamics* (Prentice-Hall, Englewood Cliffs, NJ, 1962).
14. Our results on a quantitative calculation of the flow field resulting from lateral current gradients that exist on the surface of the electrode as a result of either electrodeposited colloidal particles or scratches or defects in the ITO layer will be published elsewhere (M. Trau, D. A. Saville, I. A. Aksay, unpublished results).
15. V. Fleury, J. H. Kaufman, D. B. Hibbert, *Nature* **367**, 435 (1994); M. Wang, W. J. P. van Enkevort, N. Ming, P. Bennema, *ibid.*, p. 438; C. Livermore and P. Wong, *Phys. Rev. Lett.* **72**, 3847 (1994).
16. This work was supported by the U.S. Air Force Office of Scientific Research and the Microgravity Science and Applications Division of the National Aeronautics and Space Administration. Partial support for M.T. was provided by the Fulbright Commission. We acknowledge discussions with A. B. Bocarsly.

29 January 1996; accepted 13 March 1996

Galileo Gravity Results and the Internal Structure of Io

J. D. Anderson, W. L. Sjogren, G. Schubert

Doppler data generated with the Galileo spacecraft's radio carrier wave were used to measure Io's external gravitational field. The resulting triaxial field is consistent with the assumption that Io is in tidal and rotational equilibrium. The inescapable conclusion is that it has a large metallic core. If the core is a eutectic mixture of iron and iron sulfide, it comprises 20.2 ± 7.4 percent of the satellite's total mass with a radius that is about 52 percent of Io's mean radius of 1821.3 kilometers; if the core is pure iron, it comprises 10.5 ± 3.7 percent of the total mass with a radius of about 36 percent of the mean radius.

Jupiter is the largest planet in the solar system, almost 318 times more massive than Earth. Its gravitational field dominates the forces on its four largest satellites, discovered by Galileo in 1610. Io, its innermost Galilean satellite, is in orbital resonance with two other Galilean moons, Ganymede and Europa, and as a consequence, the tides raised on Io by Jupiter frictionally heat the satellite and produce an enhanced surface heat flow and active volcanic plumes (*1*). Io is covered by flows of sulfur, sulfur compounds, and silicates. Its mean density of 3529 kg m^{-3} and rugged topography suggest an interior composed of silicates, similar to the interiors of the Earth and its moon, as well as heavier metals.

Io is roughly the same size as Earth's moon (mean radius of 1821.3 km, compared with a lunar radius of 1738 km); however, its proximity to Jupiter and its rapid rotation (period of 1.769 days, compared with the lunar rotation of 27.3217 days) distinguishes it from our moon. Most significantly, the rotational and tidal forces on Io are 220 times larger than similar forces on Earth's moon. Consequently, although it is incorrect to assume that Earth's moon can be approximated by a fluid body in hydrostatic equilibrium, it is a good first-order approximation for Io. Deviations from equilibrium, which are responsible for frictional heating, are of higher order and are not directly detectable from flyby data.

All this was known before the Galileo mission from a combination of ground-based observations and data from the Pioneer and Voyager missions to Jupiter. However, no other spacecraft had flown as close to Io as did the Galileo spacecraft on 7 December 1995 (*2*). By analyzing radio Doppler data generated during the flyby, we measured the tidal component of Io's gravitational field (Fig. 1), and by interpreting this measurement under the assumption of rotational and tidal equilibrium, we modeled the interior structure of the satellite. These results are relevant to studies of solar system formation and comparative planetology, including that of Earth. The interior properties that we determined can be combined with previously known surface properties to gain a better understanding of how Io evolved and how it reached its present state. For example, the surface observations tell us that sulfur is present in abundance, and volcanic activity tells us that it is abundant in the interior as well. The Galileo discovery that Io has a large metallic core suggests that iron and, because of the abundance of sulfur, iron sulfide have separated from the lighter silicates to produce a differentiated satellite. Io must have been heated sufficiently during its evolution for differentiation to have occurred.

Io and Earth are the only bodies in the solar system for which a metallic core has been detected directly, by means of seismic waves for Earth and measurements of the gravitational field for Io. Given their relative locations in the solar system, this remarkable similarity must be accounted for in theories of solar system origin and evolution.

The Galileo spacecraft's telecommunication system was limited by the loss of a high-gain antenna that failed to unfurl before arrival at Jupiter (*3*). During the Io flyby, radio signals in the S band (2.3 GHz or 13-cm wavelength) were transmitted to Earth by a low-gain antenna with a temperature-controlled crystal oscillator (USO) (*3*) for frequency reference. The Deep Space Network (DSN) compensated for the low signal-to-noise ratio by tracking the spacecraft with their 70-m antennas in California, Australia, and Spain. They generated radio Doppler data from the carrier

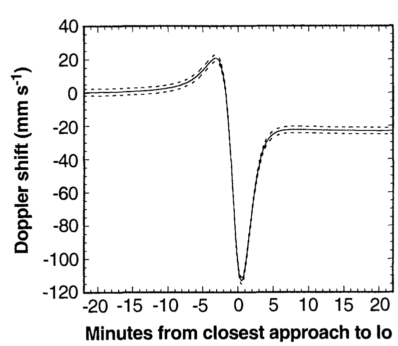

Fig. 1. Plot of the C_{22} Io gravity signal (solid line) detected in the USO Doppler data near the closest approach to Io. Doppler frequency shift is plotted according to the formula $c\Delta\nu/\nu$, where $\Delta\nu$ is the Doppler frequency shift in hertz, ν is the spacecraft's S-band transmitter frequency, and the speed of light $c = 2.998 \times 10^{11}$ mm s^{-1}. The dashed lines represent the ±2 mm s^{-1} standard error of the data.

J. D. Anderson and W. L. Sjogren, Jet Propulsion Laboratory, California Institute of Technology, Pasadena, CA 91109–8099, USA.
G. Schubert, Department of Earth and Space Sciences, Institute of Geophysics and Planetary Physics, University of California, Los Angeles, CA 90095–1567, USA.

wave in a format of discretely sampled cycles referenced to hydrogen masers (4).

The USO was inherently less stable than atomic frequency standards, so the DSN sometimes generated phase-coherent Doppler data, using the spacecraft's transponder and the DSN's three 70-m stations. To assure reliable telemetry during the Io flyby, the Galileo Project did not authorize collection of coherent data. The limited coherent data that were generated, although produced at times when the spacecraft was too far from Io to reveal a gravity signal, did provide a stable baseline for the USO data. Because the DSN was tracking the spacecraft during the Io flyby, we were able to use the USO data to determine the gravity field.

The data used in our analysis started with coherent Doppler data on 4 December 1995 at 01:52:13 [all times are Universal Time Coordinated (UTC) at Earth reception of the Galileo signal] and ended with USO data on 7 December 1995 at 20:59:30, about 2 hours before the start of data relayed from the Galileo atmospheric probe (2). The Doppler starting time was early enough to assure a good orbit determination during the Io flyby (closest approach at 18:38:00). Two criteria determined the ending time. First, the data ended before a propulsion burn at about 01:19 on 8 December that inserted the spacecraft into the desired Jupiter orbit. Inclusion of data during the propulsion maneuver would have introduced troublesome nongravitational forces. Second, although the USO was relatively immune to environmental effects, it did experience a significant shift in frequency as the radiation dose from Jupiter's magnetospheric particles increased. Any USO data taken after the selected ending time would have seriously biased the orbit determination and consequently the gravity results.

The reduced data for the experiment were Doppler frequency data. Frequency data were defined as the difference in cycle count at two times divided by the time interval. Most of the reduced frequency data were sampled in 60-s intervals, but near the closest approach to Io, for an interval of about 2 hours, the USO data were sampled in 10-s intervals. This sampling strategy suppressed the high-frequency Fourier noise components (low-pass filter) and, in addition, assured adequate resolution of the gravity signal during the flyby.

We used the Orbit Determination Program (ODP) of the Jet Propulsion Laboratory (JPL) to fit the radio Doppler data by nonlinear weighted least squares (5) (Fig. 2). A total of 23 parameters were adjusted to find the local minimum of the weighted residuals. The parameters consisted of the six Cartesian position and velocity coordinates of the spacecraft; six similar Cartesian

Table 1. Gravity results from Galileo on 7 December 1995 and from the Pioneer and Voyager missions.

Parameter	Galileo	Pioneer and Voyager
C_{22} (Io)	$(559 \pm 27) \times 10^{-6}$	None
GM (km^3 s^{-2})		
System	126,712,752 $\pm$ 40	126,712,767 $\pm$ 100
Jupiter	126,686,527 $\pm$ 40	126,686,537 $\pm$ 100
Io	5959.91 $\pm$ 0.28	5961 $\pm$ 10
Europa	3196.81 $\pm$ 0.69	3200 $\pm$ 10
Ganymede	None	9887 $\pm$ 3
Callisto	None	7181 $\pm$ 3
J_2 (Jupiter)	None	$(14736 \pm 1) \times 10^{-6}$
J_4 (Jupiter)	None	$(-587 \pm 5) \times 10^{-6}$
J_6 (Jupiter)	None	$(31 \pm 20) \times 10^{-6}$

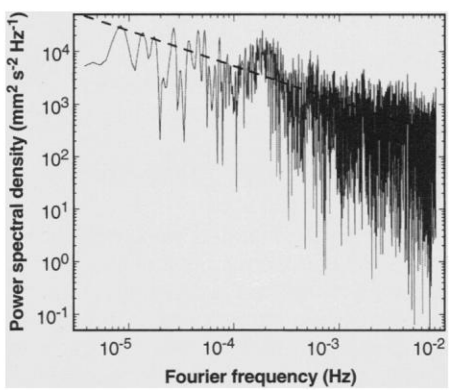

Fig. 2. Estimate of power spectral density for combined coherent and noncoherent USO Doppler frequency (f) residuals. The dashed line represents solar plasma noise (Fourier frequency dependence $f^{-2/3}$) (12). All significant systematic trends have been removed by the 23-parameter fit. The variance on the residuals, equal to the integral of the spectrum over the entire bandwidth of the data, is 6.455 mm^2 s^{-2}, and the corresponding standard error is 2.54 mm s^{-1}. In a narrower high-frequency band starting at the lower limit for the Io gravity signal at about 2.78 $\times$ 10^{-4} Hz and extending to the high-frequency cutoff, the standard error is 2.17 mm s^{-1}.

coordinates for Io's ephemeris (orbit); three mass values (gravitational constant G times mass M) for the Jupiter system, Io, and Europa, respectively; the Io gravitational coefficients J_2 and C_{22} (6); and six polynomial coefficients that fit the drift in the USO by two quadratic polynomials (spacecraft time was an independent variable). The spacecraft and Io orbits were numerically integrated at each iteration in the nonlinear process. All other dynamical and geodetic parameters were fixed at currently accepted values (7).

The coefficient J_2 could not be determined independently of Io's GM and C_{22}, so we imposed the hydrostatic constraint that J_2 is exactly $10/3$ of C_{22}. The adjustment of Europa's mass was included when we saw a clear signal in the USO Doppler residuals near the spacecraft's closest approach to Europa. The removal of this signal required a reduction in Europa's mass of 0.19%, as determined by the Pioneer and Voyager flybys, consistent with the previous error of 0.38% (8). Not all components of Io's ephemeris could be determined from a single flyby, so we introduced prior information (9) in the form of a covariance matrix determined from ground-based observations (10). The Galileo radio Doppler data increased Io's orbital radius by 9.6 $\pm$ 4.2 km, and the adjustment to orbital velocity of -396 ± 130 mm s^{-1} left Io's total orbital energy and orbital angular momentum unaffected.

The two quadratic polynomials for the USO drift were assumed to be independent. The first started at the ODP epoch of 4 December 01:52:02 and ended 16 min after closest approach to Io. This polynomial revealed a decrease in the USO frequency of 46 mHz over the 89-hour interval. At Galileo's transmitted frequency of 2.3 GHz, this decrease amounted to a change in fractional frequency $\Delta\nu/\nu$ of 1.6×10^{-11}, well within the limits of plausibility for an inherent random walk in the crystal's frequency (3). The ODP is fully relativistic, so the gravitational redshift was accounted for. The second polynomial started where the first one stopped and continued for about 2 hours until the last Doppler measurement in the fit. We extended the fit this far because the frequency drift was sufficiently linear. The USO frequency increased by 660 mHz ($\Delta\nu/\nu = 2.9 \times 10^{-10}$) over the last 2 hours, as a result of the radiation dose to the crystal.

The Io flyby [at 15.0 km s^{-1}, an altitude of 897 km, and nearly in Io's equatorial plane (closest approach at latitude $-8.5°$ and west longitude 101.1°)] and the Europa flyby (at a distance of 32,958 km at 14:00:54) yielded improvements on previous estimates of a determination of Io's C_{22} and both satellites' value of GM. The GM for the Jupiter system and for Jupiter alone [obtained by subtracting the four Galilean satellite masses from the system mass (8)] were also improved (Table 1). Masses derived from the GM determinations depend on G, for which the currently accepted value is $(6.67259 \pm 0.00085) \times 10^{-20}$ km^3 s^{-2} kg^{-1} (11). This value yields a mass of

Table 2. Two-layer Io models. Three values of C_{22} are the inferred value from the Doppler data and its $\pm 1\sigma$ variations; ρ_c = 5150 and 8090 kg m^{-3} for Fe-FeS and Fe core models, respectively (*15*).

C_{22}	C/MR^2	Axis dimensions		Fe-FeS core		Fe core	
		$(a-c)/c$	$(b-c)/c$	r_c/R	m_c/M	r_c/R	m_c/M
532×10^{-6}	0.371	7.681×10^{-3}	1.920×10^{-3}	0.576	0.279	0.397	0.143
559×10^{-6}	0.378	7.897×10^{-3}	1.974×10^{-3}	0.517	0.202	0.357	0.105
586×10^{-6}	0.386	8.113×10^{-3}	2.028×10^{-3}	0.447	0.130	0.310	0.068

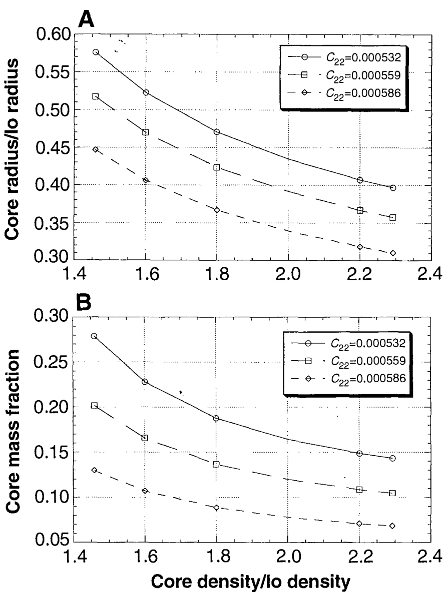

Fig. 3. (**A**) Ratio of core radius to Io radius (r_c/R) and (**B**) the core mass fraction (m_c/M) versus the ratio of core density to mean density ($\rho_c/\bar{\rho}$), with C_{22} as a parameter. The ratio $\rho_c/\bar{\rho}$ is assumed to vary between 1.46 and 2.29 (*15*).

$(8.9319 \pm 0.0012) \times 10^{22}$ kg for Io, $(4.7910 \pm 0.0012) \times 10^{22}$ kg for Europa, and $(1.89861 \pm 0.00024) \times 10^{27}$ kg for Jupiter (*12*). The ratio of the mass of the sun to the mass of the entire Jupiter system is used in the development of planetary ephemerides (*7*); its improved value is 1047.34873 ± 0.00033. Improved mean densities for Io and Europa are 3529.4 ± 1.3 and 2984 ± 46 kg m^{-3}, respectively.

A synchronously rotating satellite in tidal and rotational equilibrium forms a triaxial ellipsoid with dimensions a, b, and c ($a > b > c$). The long axis is along the planet-satellite line, and the short axis is parallel to the rotation axis. The distortion of the satellite depends on the magnitude of the rotational and tidal forcing and the distribution of its mass with radius. The distortion of the satellite and its internal mass distribution determine the satellite's gravitational field (*13*). The gravitational coefficient C_{22} is related to the difference in the equatorial moments of inertia by

$$C_{22} = \frac{B-A}{4MR^2} \qquad (1)$$

where the ellipsoidal satellite's principal moments of inertia are A, B, and C ($C > B > A$); the satellite's total mass is M, and its mean radius is R. For a body in rotational and tidal equilibrium, C_{22} is related to the rotational response parameter q_r by

$$C_{22} = \frac{3}{4}\alpha q_r \qquad (2)$$

where α is a dimensionless response coefficient that depends on the distribution of mass within the satellite (α = ½ for constant density), and q_r is the ratio of centrifugal to gravitational acceleration at the equator ($q_r = 1.7123 \times 10^{-3}$ for Io). Given C_{22} and q_r, we can determine α from Eq. 2, and the satellite's axial moment of inertia C follows from

$$\frac{C}{MR^2} = \frac{2}{3}\left[1 - \frac{2}{5}\left(\frac{4-3\alpha}{1+3\alpha}\right)^{1/2}\right] \qquad (3)$$

From Eqs. 2 and 3, $\alpha = 0.435$ and $C/MR^2 = 0.378$ for the nominal value of $C_{22} = 559 \times 10^{-6}$ determined from the Galileo Doppler data.

The axial moment of inertia provides a direct constraint on the internal mass distribution. Consistent with C_{22}, we assume a simple two-layer model for Io consisting of a core of radius r_c and density ρ_c surrounded by a mantle of density ρ_m. The known mean density $\bar{\rho}$ for the two-layer model is

$$\bar{\rho} = \left(\frac{r_c}{R}\right)^3 (\rho_c - \rho_m) + \rho_m \qquad (4)$$

and the axial moment of inertia can be determined from

$$\frac{C}{MR^2} = \frac{2}{5}\left[\frac{\rho_m}{\bar{\rho}} + \left(1 - \frac{\rho_m}{\bar{\rho}}\right)\left(\frac{r_c}{R}\right)^2\right] \qquad (5)$$

Even for the simple two-layer model, the two fundamental physical parameters ρ_c and r_c are not determined uniquely: there are two equations (Eqs. 4 and 5) and three unknown parameters (ρ_c, r_c, and ρ_m). Therefore, we parameterize the interior models with $\rho_c/\bar{\rho}$ as an independent variable and r_c/R and $\rho_m/\bar{\rho}$ as the two dependent variables. For an assumed value of $\rho_c/\bar{\rho}$, Eq. 4 yields $\rho_m/\bar{\rho}$ in terms of r_c/R; then, Eq. 5 yields the ratio r_c/R. The core mass fraction follows from

$$\frac{m_c}{M} = \left(\frac{r_c}{R}\right)^3 \left(\frac{\rho_c}{\bar{\rho}}\right) \qquad (6)$$

Basically, the total mass and inferred moment of inertia from the Doppler data analysis, plus the known mean radius, determine the mass and radius of the core as a function of $\rho_c/\bar{\rho}$ (Table 2).

Uncertainty in the actual value of $\rho_c/\bar{\rho}$ results in a range of possible values for core size and mass (Fig. 3). The theory for the equilibrium distortion of Io allows determination of the ellipsoidal shape of these models (Table 2). These values are independent of the choice of $\rho_c/\bar{\rho}$ and compare well with the determination of Io's shape from Voyager 1 imaging data (*14*).

Although lack of knowledge of the chemical composition of Io's core precludes us from deriving the exact size and mass, the conclusion that Io has a large metallic core is robust. The gravitational signal of the core was unambiguously detected during the Galileo flyby of Io. In comparison, there is yet no certain observational detection of a lunar core, which is at most about 20% of the radius of Earth's moon.

REFERENCES AND NOTES

1. For a description of Io and other Jupiter satellites, see D. Morrison, Ed., *Satellites of Jupiter* (Univ. of Arizona Press, Tucson, 1982); J. A. Burns and M. S. Matthews, Eds., *Satellites* (Univ. of Arizona Press, Tucson, 1986).
2. An overview of the Galileo mission, including a description of the spacecraft configuration (orbiter and probe), can be found in T. V. Johnson and C. M. Yeates, *Space Sci. Rev.* **60**, 3 (1992).
3. J. D. Anderson *et al.* [*Space Sci. Rev.* **60**, 591 (1992)] give a description of the Galileo gravitational experiments for all phases of the mission. The radio propagation experiments and a description of radio instrumentation and measurement techniques are discussed in H. T. Howard *et al.*, *Space Sci. Rev.* **60**, 565 (1992). The main spacecraft antenna that failed to unfurl was a 4.8-m paraboloid attached to the spinning portion of the spacecraft and aligned with the axis of rotation. The crystal oscillator, called the Ultrastable Oscillator (USO) by the Jet Propulsion Laboratory (JPL), was a spare from the Voyager mission. For Doppler integration times $\tau < 1$ s, the USO frequency was dominated by white phase noise. Between τ = 1 and 300 s, the frequency noise was white with a $\Delta\nu/\nu$ standard error of 10^{-12}. For $\tau >$ 300 s, the frequency random-walked such that the frequency error was proportional to $\tau^{1/2}$, consistent with our data analysis.
4. We have placed the data in the public domain by transferring all data files used in our analysis to nine-track magnetic tape and sending copies to the National Space Science Data Center, Goddard Space Flight Center.
5. T. D. Moyer, *Tech. Rep. TR 32-1527* (Jet Propulsion Laboratory, Pasadena, CA, 1971); J. D. Anderson, in *Experimental Gravitation*, B. Bertotti, Ed. (Academic Press, New York, 1974), pp. 163–199. The 1σ error on each Doppler velocity measurement was assumed to be 2 mm s^{-1} for both USO data and coherent Doppler data sampled at 60 s. For the 2 hours of USO data sampled at 10 s, the 1σ error was increased by a factor of $\sqrt{6}$. An ODP algorithm, applied automatically, increased the Doppler error at lower elevation angles with respect to the station's horizon.
6. For the standard spherical harmonic representation of the gravitational potential, see, for example, W. M. Kaula, *Theory of Satellite Geodesy* (Blaisdell, Waltham, MA, 1966). The coefficients J_2 and C_{22} give the contributions to the gravitational potential of the spherical harmonics of degree l and order m for

l = 2, m = 0 and l = 2, m = 2, respectively.
7. P. K. Seidelmann, Ed., *Explanatory Supplement to the Astronomical Almanac* (University Science Books, Mill Valley, CA, 1992). All orbits and station coordinates were referenced to the J2000 system with the latest JPL Lunar and Planetary Development Ephemeris (DE403). Models for the Earth's polar motion and nonuniform rotation were provided by the DSN. All Io gravity coefficients, except for the two that respond to rotation and tides (J_2 and C_{22}), were fixed at zero. We justified setting them to zero by obtaining a few fits to the Doppler data with other second-degree and -order and third-degree and -order coefficients. Our interpretation of these fits indicated that the amplitudes of nonhydrostatic components were no greater than that of noise.
8. A celestial mechanics experiment, similar to the Galileo experiment discussed here, was included on Pioneer 10 and 11 but not on Voyager. Previous results on the gravitational field of the Jupiter system can be found in G. W. Null, J. D. Anderson, S. K. Wong, *Science* **188**, 476 (1975); J. D. Anderson, in *Jupiter*, T. Gehrels, Ed. (Univ. of Arizona Press, Tucson, 1976), pp. 113–121; G. W. Null, *Astron. J.* **81**, 1153 (1976); J. K. Campbell and S. P. Synnott, *ibid.* **90**, 364 (1985). Because of the close Galileo flybys of Io and Europa, our recommended standard errors are considerably smaller than earlier realistic errors.
9. B. D. Tapley, in *Recent Advances in Dynamical Astronomy*, B. D. Tapley and V. Szebehely, Eds. (Reidel, Dordrecht, 1973), pp. 396–425.
10. R. A. Jacobson developed satellite ephemerides for the Galileo Project in support of the Navigation Team. He numerically integrated the four Galilean satellites and fit ground-based astrometric data, including satellite mutual events. His force model included the best available Jupiter gravity parameters (*8*). He included 33 parameters in the fit, including the initial position and velocity for the four Galilean satellites, five *GM* values for the satellites and the Jupiter system, J_2 and J_4 for Jupiter, and the right ascension and declination of Jupiter's pole. He made small corrections to the five *GM* values but left the Jupiter gravity parameters and the pole position unchanged from their spacecraft flyby values. The fitting model was fully relativistic, consistent with the ODP. Relativistic terms in the satellite orbits are important for consistency but are too small to provide tests of general relativity.
11. E. R. Cohen and B. N. Taylor, *Rev. Mod. Phys.* **57**, 1121 (1987).
12. Formal error estimates from the least-squares covariance matrix were based on an assumption of independent measurements drawn from a Gaussian noise distribution. The Galileo Doppler frequency data were Gaussian, but their power spectral density followed an $f^{-2/3}$ law arising from propagation of the radio carrier wave through solar plasma (Fig. 2). R. Woo and J. W. Armstrong [*J. Geophys. Res.* **84**, 7288 (1979)] have shown that this distribution is the expected noise spectrum for a radio wave passing more than 20 solar radii (5.5°) from the sun and subject to a one-dimensional Kolmogorov electron density spectrum with a spectral index of 5/3. The variance of spectral estimates of a signal roughly follows the same power-law dependence as does the noise spectrum, so the Galileo gravity signals were more accurate when determined at higher Fourier frequencies. Our data weighting, with an assumed variance approximately equal to the variance of the Doppler residuals (4 mm^2 s^{-2}), was about right for the Io and Europa gravity signals, where the peak Fourier components were around 2×10^{-3} Hz; however, it was too optimistic for the lower frequency Jupiter mass signal. We therefore retained the formal errors for the satellite gravity parameters but increased the formal Jupiter mass error by a factor of 3. Consequently, all errors adopted for this report were our best estimates of realistic standard error.
13. For example, W. M. Kaula, *An Introduction to Planetary Physics: The Terrestrial Planets* (Wiley, New York, 1968); W. B. Hubbard and J. D. Anderson, *Icarus* **33**, 336 (1978); S. F. Dermott, *ibid.* **37**, 310 (1979); V. N. Zharkov, V. V. Leontjev, A. V. Kozenko, *ibid.* **61**, 92 (1985).
14. M. Davies *et al.*, *Celestial Mech. Dyn. Astron.* **53**, 377 (1992). The principal axes are a = 1830.0 km, b = 1818.7 km, and c = 1815.3 km, all with uncertainties of 0.2 km. The error characteristics of an elliptical shape determination can be derived from an assumed continuous distribution of radius measurements. For the flattening $(a - c)/c$, the error is equal to $\sqrt{8}$ times the fractional error in each independent radius measurement (we assume 0.2/1821 for Io). Using the published axes and this error result, we obtain $(a - c)/c = (8.10 \pm 0.31) \times 10^{-3}$ and $(b - c)/c = (1.87 \pm 0.31) \times 10^{-3}$. These values and their estimated uncertainties are consistent with Table 2.
15. M. Segatz, T. Spohn, M. N. Ross, G. Schubert, *Icarus* **75**, 187 (1988); M. Wienbruch and T. Spohn, *Planet. Space Sci.* **43**, 1045 (1995).
16. This experiment was coordinated at JPL by the Galileo Radio Science Support Team (R. G. Herrera, team leader). The radio Doppler data were generated with the support of the Office of Tracking and Data Acquisition and the DSN. The data analysis depended on the availability of software and personnel of the Galileo Project Navigation Team (W. E. Kirhofer, team leader). We thank all concerned for their help and advice. We also thank E. L. Lau for generating plots from ODP computer files. The research described here was carried out by JPL, California Institute of Technology, and was sponsored by the Galileo Project through an agreement with the National Aeronautics and Space Administration.

7 March 1996; accepted 8 April 1996

Juvenile Skeletal Structure and the Reproductive Habits of Dinosaurs

Nicholas R. Geist and Terry D. Jones

Skeletal ontogeny in extant archosaurians (crocodilians and birds) indicates that the morphology of the perinatal pelvic girdle is an indicator of overall developmental maturity [that is, altriciality (nestbound) versus precociality (mobile and relatively independent)]. Comparison of the skeletal anatomy of perinatal extant archosaurians and perinatal dinosaurs suggests that known dinosaur hatchlings were precocial. These data are consistent with the overall similarity in nesting behavior of dinosaurs and modern crocodilians.

Fossils of juvenile dinosaurs can provide key information regarding dinosaur life history and physiology. To evaluate whether hatchling dinosaurs were altricial or precocial, we examined the skeletal structure in a variety of extant, perinatal precocial birds [emu (*Dromaius*), Mallee-Fowl (*Leipoa*), ostrich (*Struthio*), brush turkey (*Talegalla*)], perinatal altricial birds [macaw (*Ara*), cockatoo (*Cacatua*), eagle (*Haliaeetus*), starling (*Sturnus*)], and perinatal crocodilians (*Alligator*, *Caiman*) (all crocodilians are precocial at birth) and compared their characteristics with the skeletal features of perinatal dinosaurs (*1*).

This comparison reveals that the extent of ossification of the pelves at hatching may be a reliable indicator of the altricial or precocial nature of archosaurian neonates. Specifically, the pelves of late-fetal crocodilians and precocial birds are more ossified than those of altricial birds (Fig. 1 and Table 1) (*2*). This observation is consistent with the structure of the major locomotor muscles of the hindlimb, many of which originate from the pelvic girdle in both crocodilians and birds. Juveniles that are active cursors immediately upon hatching require a rigid, stable site of origin for limb musculature. In contrast, pelves of perinatal altricial birds are poorly ossified. However, even altricial juveniles become active within the nest in a matter of days after hatching, and postnatal ossification of the pelvic girdle is relatively rapid. Nearly complete ossification may take place within the first week. Consequently, if a fossilized embryo with well-ossified pelvic elements can be reliably identified, this criterion for distinguishing altricial from precocial neonates may be applied with some assurance. Significantly, the pelvic girdles of embryonic *Maiasaura* and *Orodromeus* (*1*), as well as all other known dinosaur embryos, including *Hypacrosaurus* (Ornithischia) (*3*), *Oviraptor* (Theropoda) (*4*), and *Therizinosaurus* (Segnosauria) (*5*), were apparently well ossified. These observations indicate that precociality was possibly widespread in dinosaurs.

Earlier hypotheses regarding altriciality in certain ornithischian dinosaurs were based on long bone epiphyseal ossification (*1*, *6*). Long bone elongation in all extant fetal archosaurians (birds and crocodilians) is centered in a massive cartilaginous cone at each end of the shaft. The cartilaginous cone consists of a cap of articular cartilage that overlies a distinct growth zone of proliferating chondrocytes (cartilage-producing cells). These chondrocytes, in turn, rest above a large, temporary mass of hyaline cartilage.

At the perinatal stage in all extant archosaurians, whether altricial or precocial, the growth zone differentiates into distinct regions of proliferating and hypertrophying chondrocytes. The chondrocytes themselves are superficial to a region of calcified cartilage that is interspersed with spongy

Department of Zoology, Oregon State University, Corvallis, OR 97331, USA.